arXiv:1410.2359v1 [physics.ao-ph] 9 Oct 2014

Role of mesoscale eddies in transport of Fukushima-derived cesium isotopes in the ocean

M.V. Budyansky, V.A. Goryachev, D.D. Kaplunenko, V.B. Lobanov, S.V. Prants, A.F. Sergeev, N.V. Shlyk, M.Yu. Uleysky

V.I.Il'ichev Pacific Oceanological Institute of the Far-Eastern Branch of the Russian Academy of Sciences, 43 Baltiyskaya st., 690041 Vladivostok, Russia
URL: http://dynalab.poi.dvo.ru

Abstract

We present the results of *in-situ* measurements of ^{134}Cs and ^{137}Cs released from the Fukushima Nuclear Power Plant (FNPP) collected at surface and different depths in the western North Pacific in June and July 2012. It was found that 15 month after the incident concentrations of radiocesium in the Japan and Okhotsk seas were at background or slightly increased level, while they had increased values in the subarctic front area east of Japan. The highest concentrations of ^{134}Cs and ^{137}Cs up to 13.5 $\pm$ 0.9 and 22.7 $\pm$ 1.5 Bq m^{-3} have been found to exceed ten times the background levels before the accident. Maximal content of radiocesium was observed within subsurface and intermediate water layers inside the cores of anticyclonic eddies (100 – 500 m). Even slightly increased content of radiocesium was found at some eddies at depth of 1000 m. It is expected that convergence and subduction of surface water inside eddies are main mechanisms of downward transport of radionuclides. *In situ* observations are compared with the results of simulated advection of these radioisotopes by the AVISO altimetric velocity field. Different Lagrangian diagnostics are used to reconstruct the history and origin of synthetic tracers imitating measured seawater samples collected in each of those eddies. The results of observations are consistent with the simulated results. It is shown that the tracers, simulating water samples with increased radioactivity to be measured in the cruise, really visited the areas with presumably high level of contamination. Fast water advection between anticyclonic eddies and convergence of surface water inside eddies make them responsible for spreading, accumulation and downward transport of cesium rich water to the intermediate depth in the frontal zone.

Keywords: Fukushima accident, radiocesium observation, Lagrangian modelling, mesoscale eddies

1. Introduction

The great Tohoku earthquake of magnitude 9.0 on 11 March 2011 followed by the tsunami inflicted heavy damage on the Fukushima Nuclear Power Plant (FNPP) due to overheating the reactors and hydrogen explosions. Large amount of radioactive water leaked directly into the ocean (Tsumune et al., 2012; Kanda, 2013). Moreover, the radioactive pollution of the sea was also caused by atmospheric deposition on the ocean surface (Takemura et al., 2011; Miyazawa et al., 2013). Radioactive cesium with 30.17 yr half-life for ^{137}Cs and 2.06 yr half-life for ^{134}Cs has been detected over a broad area in the North Pacific in 2011 and 2012 (Honda et al., 2012; Buesseler et al., 2012; Inoue et al., 2012a,b; Kaeriyama et al., 2013; Oikawa et al., 2013; Aoyama et al., 2013; Kameník et al., 2013; Kumamoto et al., 2014; Kaeriyama et al., 2014). ^{137}Cs is a passive tracer in seawater which can be used to study long-term circulation and ventilation of water masses in the global ocean. In particular, distribution of Fukushima-derived ^{137}Cs in the ocean would help to validate numerical circulation models and their parameters.

The area east of Japan is known as Kuroshio–Oyashio confluence zone (Kawai, 1972) or sub-

Email address: prants@poi.dvo.ru (S.V. Prants)

arctic front area. Existence of a large number of mesoscale eddies in this area should influence the transport of water contaminated with Fukushima-derived radionuclides. Among these eddies, the Kuroshio warm core rings are most energetic and long-lived ones (see, e.g., Kitano, 1974; Itoh and Yasuda, 2010a). Strong and persistent anticyclonic eddies are also observed along the Kuril Islands (Bulatov and Lobanov, 1992; Yasuda et al., 2000).

Both cyclonic and anticyclonic eddies would provide fast transport of surface water by streamers. However, because of a divergence in the cyclonic eddies one may expect upwelling of deep water and thus lower concentration of radionuclides in the surface layer. In opposite, we may expect accumulation of contaminated water in anticyclonic eddies because of convergence in their surface layer and following subduction to the deeper ocean. In addition, winter convection should increase penetration of contaminated water to deeper layers inside anticyclonic eddies in comparison with surrounding waters.

It is known that Kuroshio warm-core rings may move north-eastward toward the Kuril Islands (Lobanov et al., 1991; Bulatov and Lobanov, 1992; Yasuda et al., 1992; Itoh and Yasuda, 2010a) and thus transport trapped water with a higher cesium content to the north of the subarctic front. To prove this hypothesis we have performed a numerical modelling of tracer transport in the area east of Japan and implemented a cruise to cross major streams and eddies in the area using R/V "Professor Gagarinskiy" of the Far Eastern Branch of Russian Academy of Sciences. The cruise has been conducted from 12 June to 10 July 2012, 15 months after the accident.

We focus here on comparing the experimental results, obtained with water samples at stations in the centers of some selected anticyclonic eddies in the region, with the results of numerical simulation of spatial distribution of Fukushima-derived radionuclides. That simulation helps to explain why we have detected comparatively high cesium concentrations in the cores of some eddies and lower ones in the other eddies.

The paper is organized as follows. In section 2 we briefly present for comparison the results of previous direct observations of ^{134}Cs and ^{137}Cs in the area of the western North Pacific (Honda et al., 2012; Buesseler et al., 2012; Kaeriyama et al., 2013) where some of our sampling stations were located. Section 3 describes the cruise track, sample collection, the methods of radioactive analysis and computation. The numerical Lagrangian methods we used are based on solving advection equations for synthetic particles in an altimetric velocity field provided by AVISO. Section 4 contains the main results and a discussion. We present a table summarizing the results of our measurements of the concentration of ^{134}Cs and ^{137}Cs in seawater samples collected at different depth horizons in the broad area in the Sea of Japan, the Okhotsk Sea and the western North Pacific. Simulation results are plotted as tracking maps revealing origin and history of water masses collected at representative sampling stations where different values of concentration of ^{134}Cs and ^{137}Cs have been observed. They are compared with the corresponding measurements. In this section we analyze as well vertical cross-section of potential density anomaly, potential vorticity, distribution of cesium isotopes in surface water along the cruise track and vertical distribution of ^{134}Cs and ^{137}Cs at some selected stations. It is also discussed why measured activities of cesium differs strongly at different stations. Results are summarized in Section 5.

2. Previous observations of Fukushima-derived cesium

Before March 2011, ^{137}Cs concentration levels off Japan were 1–2 Bq m^{-3} $\simeq$ 0.001–0.002 Bq kg^{-1}, while ^{134}Cs was not detectable. Because of a comparatively short half-life time, any measured concentrations of ^{134}Cs could only be Fukushima derived. Concentrations at the FNPP discharge channels in early April 2011 was more than 50 million times greater than the preexisting ocean level of ^{137}Cs (Buesseler et al., 2012).

One month after the accident, sea-water, suspended solids and zooplankton samples were collected from the surface mixed layer and subsurface layers at a number of stations, 200–2000 km offshore from the FNPP (Honda et al., 2012). In surface water, ^{137}Cs concentrations were ranged from several times to two orders of magnitude higher than before the accident. ^{134}Cs isotope was also detected with the ratio ^{134}Cs/^{137}Cs to be about 1. The highest concentrations, from $\approx$150 Bq m^{-3} to $\approx$350 Bq m^{-3}, have been found off the FNPP ($\approx$200 km from the nuclear power plant) and Miyagi (the earthquake source). ^{137}Cs concentrations to

the east of this region in the area (146–147° E; 37–38° N) were also high (≈50–60 Bq m^{-3}). The ^{137}Cs concentrations in the Kuroshio Extension, <10 Bq m^{-3}, were unexpectantly low, because it was considered to be the main potential pathway for contaminated water to the open ocean.

The expedition of the Russian Hydrometeorological Service on R/V "Pavel Gordienko" in 24 April – 6 May 2011 (Karasev, 2012) proved increased concentration of both ^{137}Cs and ^{134}Cs in surface water along the whole Kuril Island chain (2.2–3.6 Bq m^{-3} and 1.2–2.9 Bq m^{-3}, correspondingly) but not at the southern part of the Kamchatka Peninsula, where those concentrations were 1.4 and 0.4 Bq m^{-3}, correspondingly. Such distribution of radionuclides could be explained by atmospheric transport. They also found high concentration of radionuclides in the area about 350 km east of Tohoku, where ^{137}Cs and ^{134}Cs contents were found to be up to 24 and 21 Bq m^{-3}, correspondingly.

The R/V "Ka'imikai-o-Kanaloa" cruise has been conducted in 4–18 June 2011 by (Buesseler et al., 2012) to investigate the distribution of Fukushima-derived radionuclides in seawater, zooplankton and micronectonic fishes 30–600 km offshore from the FNPP. Activities up to 325 Bq m^{-3} were found more than 600 km offshore. As to ^{137}Cs, the highest level (except for the discharge channels), 600 – 800 Bq m^{-3}, has been detected 30 km offshore. In June, Fukushima-derived Cs did not generally penetrate below 100–200 m. Over time, it is expected to find deeper penetration proving a means to study the rates of vertical mixing processes in the Pacific. Fukushima-derived isotopes have been also detected in zooplankton (with the maximal level about $5 \cdot 10^4$ Bq m^{-3} dry weight comparable with the recommended value of $4 \cdot 10^4$) and jellyfish but not in micronectonic fishes. In June 2011, the highest surface-water concentrations for both the isotopes, $3.9 \cdot 10^3$ Bq m^{-3}, have been detected in a semipermanent mesoscale eddy centered at (142.5° E; 37° N), not the nearest location to the nuclear power plant.

Results of direct observation of ^{134}Cs and ^{137}Cs in surface seawater collected from R/V "Kaiun maru" in a broad area in the western and central North Pacific in July, October 2011 and July 2012 have been reported by Kaeriyama et al. (2013). In particular, seawater samples were collected at their stations C43–C55 (26–29 July 2011) located from 35° N to 41° N along the 144° E transect with its southern edge crossing a crest of the Kuroshio Extension meander and the northern edge crossing partly the Tohoku mesoscale eddy centered at that time at (≈144° E; 38° N). That eddy is a warm-core Kuroshio ring permanently present in the region till the end of our cruise and later. It is clearly seen in an earlier simulation of Fukushima-derived radionuclides propagation (see Fig. 3b by Prants et al., 2011b) and in the present one marked by letter 'T' on the Lagrangian maps in Fig. 3. During 15 months after the accident, that eddy has interacted with a number of adjacent eddies and streamers promoting transport of contaminant water to the north, south and east. The measured ^{137}Cs concentrations at stations C43–C55 have been varied from the background level of 1.9 ± 0.4 Bq m^{-3} (station C52) to 153 ± 6.8 Bq m^{-3} (station C47). The ratio ^{134}Cs/^{137}Cs was close to 1.

3. Materials and methods

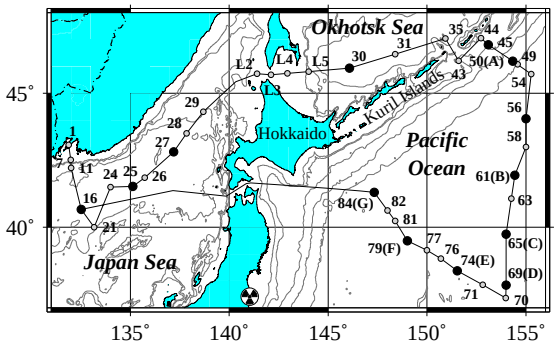

Figure 1: Locations and numbers of stations where surface (open circles) and deep seawater samples (full circles) were collected during the cruise (12 June – 10 July 2012). Letters A, B, C, D, E, F and G mark elliptic points in the centers of the corresponding mesoscale eddies to be studied. Radioactivity sign is location of the FNPP.

The cruise on the board of R/V "Professor Gagarinskiy" was conducted with the aim to collect data on the distribution of artificial radionuclides after the accident at the FNPP in the area of the Japan Sea, Sea of Okhotsk and the adjacent area of the Northwest Pacific (Fig. 1). We used standard methods to collect water and biota followed by laboratory processing and detection of ^{134}Cs and ^{137}Cs with a high-purity germanium spectrometer.

3.1. Sample collection

During the cruise, conducted from 12 June to 10 July 2012, surface water samples were col-

lected along the cruise track by a submerged pump at 54 stations. Water samples from subsurface and deep layers (100–3621 m) were taken using a CTD/Rosette sampling system at 15 stations. A volume of each water sample was 95–120 liters. Locations of stations are shown in Fig. 1. The water samples pretreatment for measurement of ^{134}Cs and ^{137}Cs isotopes was performed on board by concentrating the cesium isotopes on the selective sorbent ANFEZH (Remez, 1996; Remez and Sapozhnikov, 1996; Bandong et al., 2001) with a preliminary separation of suspended matter. Water was pumped through a filter and then through the sorbent with a flow rate around 2 liters per minute.

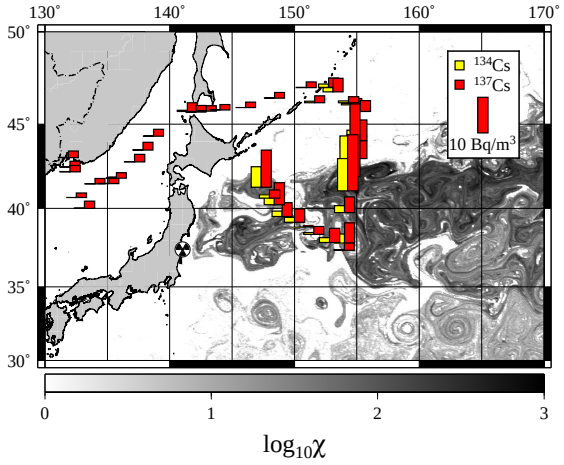

Figure 2: Simulated distribution of radionuclides concentration in the Northwest Pacific to the end of June 2012 with measured concentrations of ^{134}Cs and ^{137}Cs in Bq m^{-3} imposed. The relative simulated concentration, χ, is in a logarithmic scale.

3.2. Measurements of ^{134}Cs and ^{137}Cs in seawater

Further processing of the samples and measurements of gamma activity have been continued at the land-based laboratory at the V.I. Il'ichev Pacific Oceanological Institute in Vladivostok. Each sorbent has been dried in the oven for 3–5 hours at temperatures of 70–80 °C and then burned in a muffle furnace at temperatures of 430–450 °C during 10–15 hours. Initial sorbent of each water sample had a volume of 320 cm^3 and a weight of 80 g, while the ash in the measuring vessel for gamma spectrometry, remained after combustion of the sorbent, had a volume of 4.5–4.7 cm^3. Minimizing the sample volume is essential for gamma-spectrometric analysis as it allows decreasing a minimum detective activity. Recovery efficiency of cesium and ^{60}Co was 0.98 ± 0.02 and 0.67 ± 0.1, respectively, where errors ± 0.02 and ± 0.1 are equal to 2σ of ten ^{137}Cs and ^{60}Co labeled sea water samples processing.

Gamma activity and radioisotope composition have been determined with a gamma spectrometer with a high purity germanium detector GEM150 and a digital multi-channel analyzer DSPEC jr 2.0 (ORTEC). To reduce the background activity, the detector was placed in a lead shield with 10 cm thickness of the wall and cover and inner walls covered with a copper layer of 1 mm thickness. Integral background count rate of the detector in the shield within the energy range of 50–2990 KeV is 6.6 counts per second. We have obtained the following minimum detective activities for the measurement of 80 g ANFEZH blank sample during 160000 s: ^{134}Cs — 0.004 Bq, ^{137}Cs — 0.005 Bq and ^{60}Co — 0.014 Bq. For the spectrometer calibration we used an 80 g sorbent soaked with solution of known concentration of ^{134}Cs, ^{137}Cs and ^{60}Co after its ashing. The gamma-ray spectrum was analyzed using the software package Gamma Vision-32, version 6.09, ORTEC. True-coincidence correction factor for ^{134}Cs in our case was determined as 1.64. The ^{134}Cs to ^{137}Cs ratio was found to be 0.62 (Fig. 1s in supplementary material), whereas at the time of accident this value was equal 1. This decrease corresponds to a partial disintegration of ^{134}Cs for 15 months after the accident. All results were corrected to the sampling date.

3.3. Lagrangian simulation

To simulate propagation of Fukushima-derived radionuclides we apply in this paper the Lagrangian approach that is based on computing trajectories of tracers advected by an AVISO velocity field in accordance with the following equations:

$$\frac{dx}{dt} = u(x, y, t), \quad \frac{dy}{dt} = v(x, y, t), \qquad (1)$$

where x and y are the longitude and latitude of a tracer in geographical minutes, u and v are angular zonal and meridional components of the surface velocity expressed in minutes per day. Geostrophic velocity field, from the day of accident 11 March 2011 to the end of the cruise in the Pacific ocean area on 5 July 2012 (station 84), were obtained from the AVISO database (aviso.oceanobs.com). The

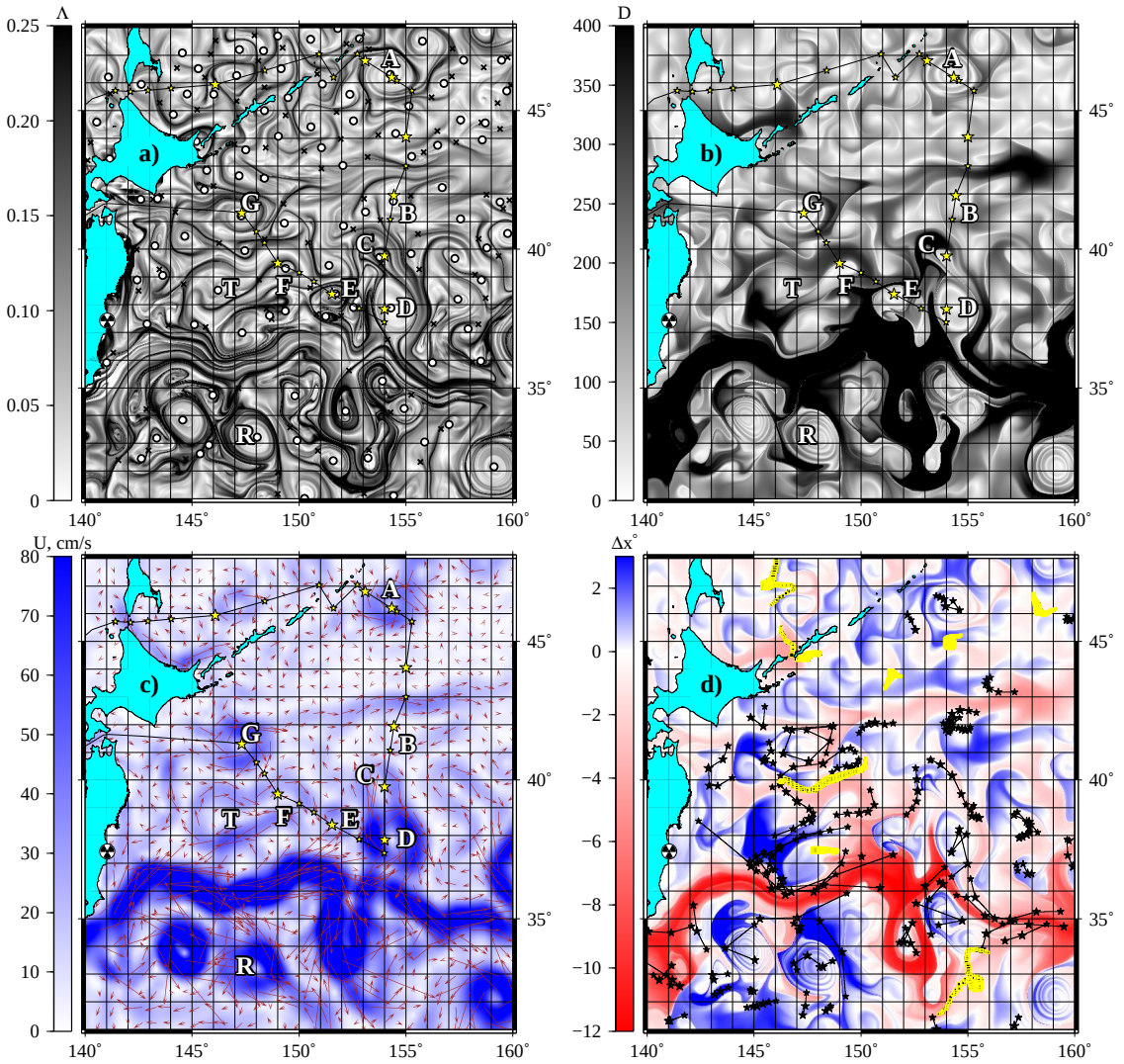

Figure 3: Anticyclonic eddies of the subarctic front A, B, C, D, E, F and G (a) on the Lyapunov map (Λ is in days^{-1}), (b) on the drift map (the absolute displacement of tracers D is in km) and (c) in the altimetric velocity field (the speed U is in cm/sec) with elliptic (circles) and hyperbolic (crosses) "instantaneous" stagnation points imposed on 28 June 2012. The ship's track and some sampling stations are shown. (d) Backward-in-time zonal drift map on 28 June 2012 with "light" ("red" online) and "dark" ("blue" online) waters passing for 15 days large distances in the west – east and the east – west directions, respectively (for interpretation of the colors in this figure, the reader is referred to the web version of this article). The values of zonal displacements of particles, $\Delta x \equiv x_f - x_0$, are given in geographic degrees. Tracks of buoys ARGOS (stars) and drifters (squares) are shown in the area for the same period of time.

data is gridded on a $1/3^\circ \times 1/3^\circ$ Mercator grid. Bicubical spatial interpolation and third order Lagrangian polynomials in time have been used to provide accurate numerical results.

When integrating Eqs. (1) forward in time, one gets an information about the fate of tracers. That is a common way to simulate the horizontal distribution pattern of radionuclides released from the FNPP (Kawamura et al., 2011; Dianskii et al., 2012; Nakano and Povinec, 2012; Dietze and Kriest, 2012; Miyazawa et al., 2013; Behrens et al., 2012; Rypina et al., 2013; Tsumune et al., 2013; Choi et al., 2013; Rossi et al., 2013; Maderich et al., 2014). We present forward-in-time simulation results in Figs. 2 and 4. In order to compute Lyapunov and other Lagrangian maps with eddies and streamers to be present in the area studied, we perform

backward-in-time integration for 15 days. The corresponding results are shown in Fig. 3. The Lagrangian maps have been shown to be useful in studying transport and mixing in different basins, from marine bays (Prants et al., 2013) and seas (Prants et al., 2011a) to the ocean scale (Prants et al., 2011b; Prants, 2013).

Our main goal in simulation is to trace out the origin and history of water samples that have been collected 15 months and later after the accident to measure the cesium concentration. To do that we seed a square 2×2 km around the location of a given sampling station with tracers and advect them backward in time in the altimetric velocity field, beginning from the date of sampling to the day of the accident. Fixing the places on a regional map, where the corresponding artificial tracers have been found for one month after the accident, we can estimate by the tracer density the probability to detect higher concentrations of Fukushima-derived radionuclides in surface seawater samples at sampling stations. The corresponding backward-in-time tracking maps aree shown in Figs. 8, 9 and 10. The simulated results are compared with the results of measurements of ^{134}Cs and ^{137}Cs.

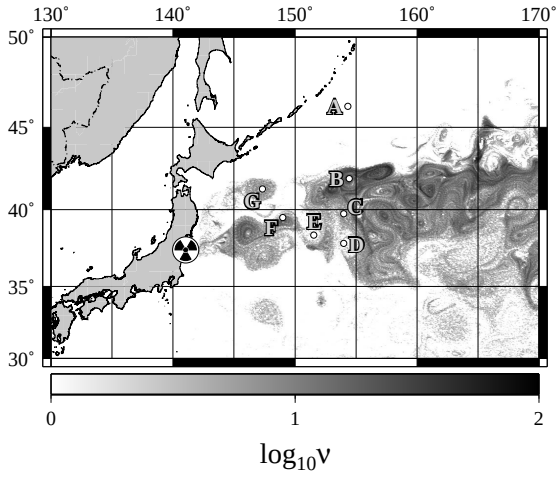

Figure 4: Simulated forward-in-time tracking map for the "radioactive" tracers distributed initially inside the box around the FNPP with the coordinates (140–144° E; 36.5–38.5° N). The map shows where those tracers have been from 24 June to 6 July 2012. Letters A, B, C, D, E, F and G mark elliptic points (circles) in the centers of the corresponding mesoscale eddies to be studied. The density of tracers, ν, is in a logarithmic scale.

The specific Lagrangian maps are used to identify eddies and transport pathways in the region. The finite-time Lyapunov exponent (FTLE) field is known to characterize quantitatively mixing of water (Pierrehumbert and Yang, 1993) and can be used, in particular, to identify eddies, streamers and fronts in irregular velocity fields in the area (Prants et al., 2012; Prants, 2013; Prants et al., 2014b,a). The FTLE is computed here by the method of the singular-value decomposition of an evolution matrix for the linearized advection equations (Prants et al., 2011a) with the help of the formulae

$$\Lambda(t, t_0) = \frac{\ln \sigma(t, t_0)}{t - t_0}, \tag{2}$$

which is the ratio of the logarithm of the maximal possible stretching in a given direction to the integration time interval $t - t_0$. Here $\sigma(t, t_0)$ is the maximal singular value of the evolution matrix. This method enables to identify accurately mesoscale eddies in altimetric velocity fields. Another means to identify eddies and transport pathways is provided by the absolute, zonal and meridional drift maps (Prants et al., 2011b, 2012, 2013, 2014b,a). The finite-time absolute displacement is a distance between final and initial positions of advected particles on the sea surface. We compute the absolute displacement and its zonal and meridional components backward in time for a large number of particles in order to identify mesoscale eddies and zonal and meridional jets to be present in the region for a given period of time. The absolute displacement, D, is simply a distance between final (x_f, y_f) and initial (x_0, y_0) positions of advected particles on the Earth sphere with the radius R

$$D \equiv R \arccos[\sin y_0 \sin y_f + \cos y_0 \cos y_f \cos(x_f - x_0)]. \tag{3}$$

Stagnation points, where the altimetric velocity is found to be zero, contain important information about the regional flow. We compute them daily, check their stability type by standard stability tests and impose them on FTLE and drift maps as circles (elliptic points) and crosses (hyperbolic points). The elliptic points, situated mainly in the centers of eddies, are those "instantaneous" stagnation points around which the motion is stable and circular. The hyperbolic points, situated mainly between and around of eddies, are unstable ones with two directions along which waters converge to such a point and another two directions along which they diverge.

4. Results and discussion

In this section we present the results of direct observations of ^{134}Cs and ^{137}Cs in surface seawater and at different depths in a broad area in the Sea of Japan, the Okhotsk Sea and the western North Pacific and discuss measured levels of the isotope concentrations. Those observations are compared with the results of numerical simulation of spatial distribution of Fukushima-derived radionuclides based on the altimetric velocity field.

4.1. Observed and simulated horizontal distribution patters of radiocesium

Concentrations of ^{137}Cs in the Japan and Okhotsk Seas have been found to be 1.4–2.3 and 1.5–1.9 Bq m^{-3}, accordingly (Table 1 in Appendix and Fig. 2), and did not exceed much pre-accident level. A slightly increased concentration of ^{134}Cs (2.4 Bq m^{-3}) was found only at one station L2 located in the northeastern Japan Sea off northern tip of the Hokkaido Island. This station was sampled in the area of the Tsushima Current which transports water contaminated by river runoff from the Honshu Island that could explain a higher concentration of ^{137}Cs. This is in accordance with observations by (Inoue et al., 2012b) which showed an increase of ^{134}Cs and ^{137}Cs concentrations in surface water transported by the Tsushima Current along the west coast of Japan to Hokkaido.

All surface water samples, collected in the Pacific Ocean, contain an increased concentration of ^{134}Cs, 0.2–11.9 Bq m^{-3}, with except of Station 76 (Table 1 in Appendix and Fig. 2). This station was taken in the warm streamer extended northward from the Kuroshio Extension jet and thus transported relatively clean water. ^{137}Cs concentrations in all samples in the western subarctic Pacific and Kuroshio – Oyashio frontal zone were in the range of 1.8–21 Bq m^{-3}. The surface water maximal ^{134}Cs and ^{137}Cs concentrations were registered in the frontal zone between stations 56–65 and stations 81–84 (Fig. 2). This confirms accumulation of surface water in the frontal zone with particular increased content in anticyclonic mesoscale eddies. Below we will discuss a role of those eddies in more details.

Solving the advection equations (1) backward in time, we have computed FTLE and drift Lagrangian maps on each cruise day. Those maps have been sent electronically to the board and used to correct the cruise track in order to cross prominent eddies in the area. Below we show simulated lateral distribution of radionuclides and compare that with cruise observations.

The initial distribution of radionuclides is supposed to be a patch with tracer concentration decreasing logarithmically with distance from the FNPP location. We advect tracers by the corresponding altimetric velocity field, starting not from the date of tsunami but from 25 March 2011, in order to take into account not only a direct release of radioactive material from the FNPP but, as well, a subsequent atmospheric deposition on the ocean surface just after the tsunami on 11 March. Variations in the initial date do not change significantly the simulation results. The concentration distribution, χ, in the end of June 2012 is shown in Fig. 2 in a logarithmic scale with measured concentrations of ^{134}Cs and ^{137}Cs imposed.

As expected, tracers in the surface layer were transported mainly along the Kuroshio Extension to the east. The concentration is larger on the north flank of the parent jet because the larger part of the initial radioactive patch was situated to the north from the eastward jet. Transport of radionuclides to the southern flank of the Kuroshio Extension may be explained partly by tracer advection from the southern part of the initial patch. Moreover, there exist another transport pathways for Fukushima-derived radionuclides. One of them, a cross-jet transport, have been studied numerically in the AVISO field by (Prants et al., 2014b) and confirmed by tracks of surface drifters released during the "Ka'imikai-o-Kanaloa" cruise (Buesseler et al., 2012) and before. The mechanism of meridional cross-jet transport, documented by (Prants et al., 2014b), is pinching off rings with contaminated water from the southern flank of the Kuroshio Extension jet. We have not found the significant impact of the initial patch's size on the concentration distribution. *In situ* observations are consistent qualitatively with the simulation: the maximal measured concentrations at the stations selected have been detected in those areas in Fig. 2 where the density of artificial tracers is really comparatively high.

4.2. Distribution of anticyclonic mesoscale eddies

The cruise track, shown on the FTLE map in Fig. 3a, b and c was chosen to cross the eddies A, B, C, D, E, F and G marked on that figure. All they are anticyclonic mesoscale eddies of the subarctic front but of different origin and history. The

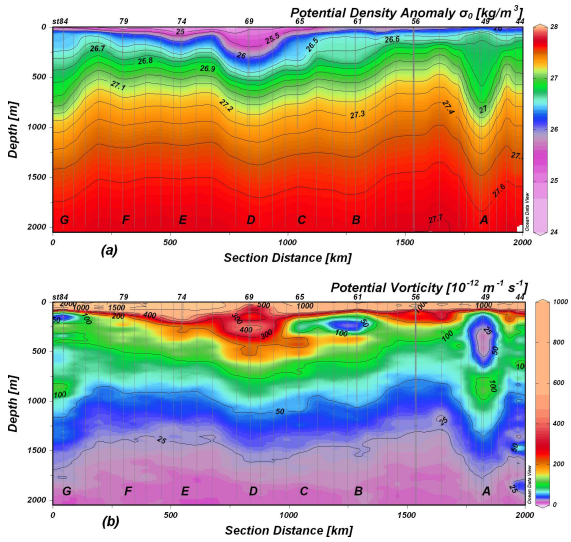

Figure 5: Vertical cross-section of (a) potential density anomaly and (b) potential vorticity along the cruise track from the central Kuril Islands (right) to Hokkaido (left). Station numbers are indicated along the top axis, locations of anticyclonic eddy centers are marked as A – G.

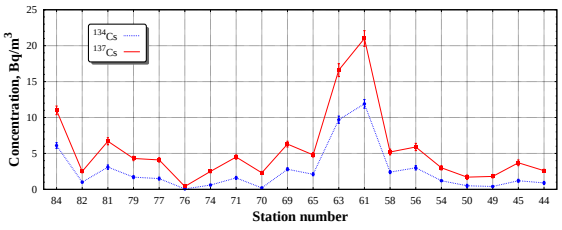

Figure 6: Distribution of cesium isotopes ^{134}Cs (dotted line) and ^{137}Cs in surface water along the cruise track in the Pacific. Locations of stations, centers of the mesoscale eddies to be studied and cruise track are shown in Fig. 1.

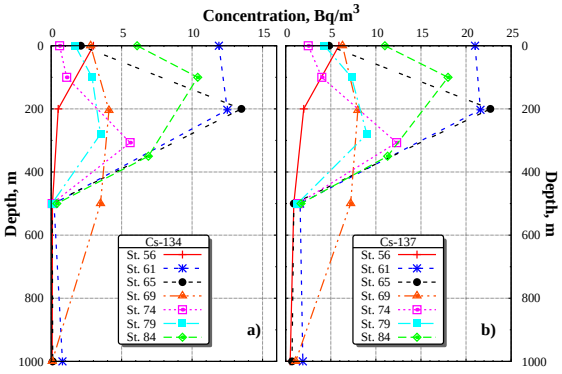

Figure 7: Vertical distribution of (a) ^{134}Cs and (b) ^{137}Cs in Bq m^{-3} for some selected stations.

eddy A is a long-lived quasi-stationary Kuril anticyclone. The eddy B appeared in the northern subarctic front area on the southern flank of a zonal eastward jet transporting waters along 42–43° N from the eastern coast of Japan (see Fig. 3d). The eddy C forms a pair along with the warm-core Kuroshio ring D that was pinched off from a Kuroshio Extension meander in the end of May 2012. Both are clearly seen on the velocity map in Fig. 3b as a vortex pair. The warm-core Kuroshio ring E was pinched off from a meander of the Kuroshio Extension jet on 10–12 June 2012 and disappeared in the middle of July. The eddy F has not been identified as a ring pinched off from the Kuroshio Extension. The eddy G, located south-east of Hokkaido, is a typical warm-core ring of the Kuroshio. It has been found to be closely related with the warm mesoscale eddy located to the south-west off the Tohoku area (the Tohoku eddy T).

The frontal Kuroshio – Oyashio zone is populated with mesoscale eddies of different sizes and lifetimes. They can be visualized on Lagrangian synoptic maps of the region computed backward in time. We seed on a fixed day 1000×1000 tracers distributed homogeneously over the region shown on the maps and integrate them backward in time for 15 days starting from 28 June 2012. The mesoscale eddies are delineated in Fig. 3a by black "ridges" of the FTLE field which are known to approximate so-called unstable manifolds of the hyperbolic trajectories (Haller, 2000) to be present in the area during the integration period, 15 days in our case. Backward-in-time drift map in Fig. 3b on 28 June 2012 shows by shadows of grey color the absolute displacements of synthetic particles, D, in km for 15 days before the date indicated. The mesoscale eddies look like patches of different color than surrounding waters. The most prominent eddies with elliptic points in their centers are also visible in the altimetric AVISO velocity field (Fig. 3c).

In the following numerical experiment tracers, distributed on 18 March 2011 over the box around the FNPP with the coordinates (140–144° E; 36.5–38.5° N), have been advected forward in time in the altimetric velocity field. In Fig. 4 we show the simulated density of tracers during the cruise period in the North Pacific region, from 24 June to 6 July 2012. The area with the Kuril mesoscale eddy A, centered at (154.33° E; 46.19° N), has not been visited during that period by potentially radioactive tracers. The measured concentrations of ^{134}Cs and ^{137}Cs at station 50 in the center of that

eddy did not exceed the background level at 0, 200, 500 and 1000 m depth. As to the other eddies of interest, the maximal radionuclide concentrations have been detected in the centers of the eddies B, (centered at 154.4° E; 41.9° N), and G, (centered at 147.3° E; 41.3° N), where the simulated density of tracers is really higher in Fig. 4. The Kuroshio rings D, centered at (154° E; 37.84° N), and E, centered at (151.5° E; 38.38° N), look like white patches on the map. It means that potentially radioactive tracers were able to visit during the simulation period their periphery but not the core.

Besides of the eddies of interest, the increased density of tracers are clearly seen in Fig. 4 at the places of the Tohoku eddy T with the center in the simulation period at (146.5° E; 38° N) and a cold-core cyclonic Kuroshio ring R, centered at (147.5° E; 33° N). As to the Tohoku eddy, it was found by Kaeriyama et al. (2013) to be strongly contaminated by ^{134}Cs and ^{137}Cs just after the accident. The increased simulated density of tracers in the cold cyclonic ring R to the south of the Kuroshio Extension means that some tracers from the initial patch could be transported southward to the parent jet and then be trapped by that eddy. We have found that the ring R was pinched off from a meander of the Kuroshio Extension jet and moved slowly to the west along its southern flank. In fact, it is a demonstration of transport of radionuclides across the strong Kuroshio Extension jet documented and studied by Prants et al. (2014b).

Concluding this section, the reader is referred to Fig. 2s in supplementary material where we show positions of those simulated tracers on 2 July 2012 that have visited just after the accident (from 11 March to 10 April 2011) two selected areas around the FNPP. The density of points in the centers of the eddies B, C and G, where the highest cesium concentrations have been detected in the cruise, is really comparatively large in this figure.

4.3. Vertical structure of the mesoscale eddies and vertical distribution of ^{134}Cs and ^{137}Cs

Results of CTD observations in the cruise demonstrate a very good correspondence with the modeled mesoscale eddy locations. Using the modeled maps of the eddy field (Figs. 3a–d) transmitted operationally on ship's board during the cruise, we managed to cross the eddies very close to their centers. The only exception was the mesoscale eddy D that was crossed along its western edge, not exactly

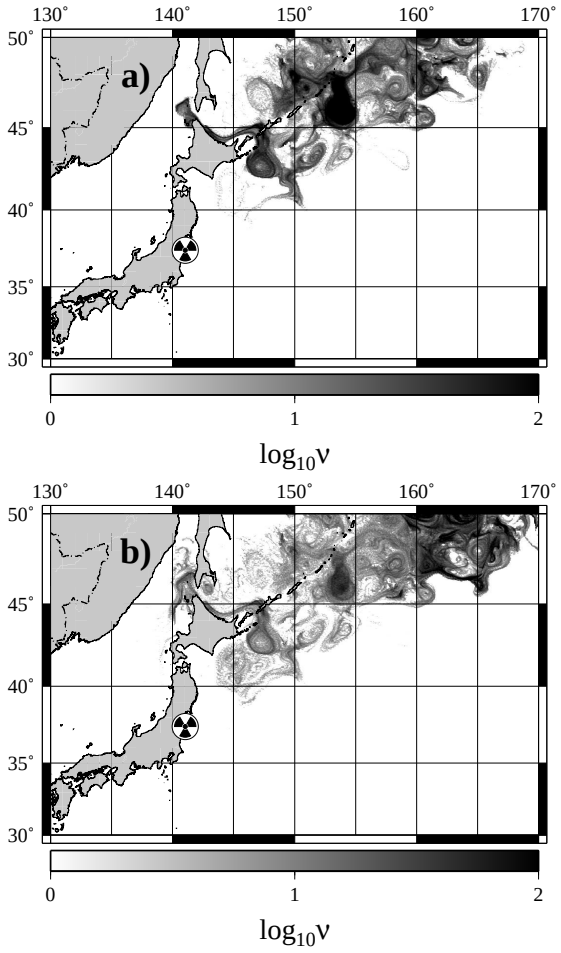

Figure 8: Backward-in-time tracking maps for tracers distributed (a) in the center of the mesoscale eddy A at station 50 and (b) at station 56, outside any eddy. The maps show where the corresponding tracers have been just after the accident, from 11 March to 10 April 2011. The density of tracers, ν, is in a logarithmic scale.

through its center. Figure 5a shows a vertical distribution of potential density anomaly along the cruise track (see Fig. 1) from the central Kuril Islands in the north (station 44) and down to the Kuroshio Extension in the south (station 70) and then to the northwest toward Hokkaido (station 84). As anticyclonic eddies contain water of lower density in their cores, their locations are clearly seen by downward deflection of isopycnal lines. All of the 7 sampled eddies can be traced down to 1000 m depth and five of them (A, B, D, F and G) can be seen down to the maximal depth of the CTD observations (2000 m). Considering a magnitude of isopycnal lines deflection, the Kuril anticyclonic mesoscale eddy A seems

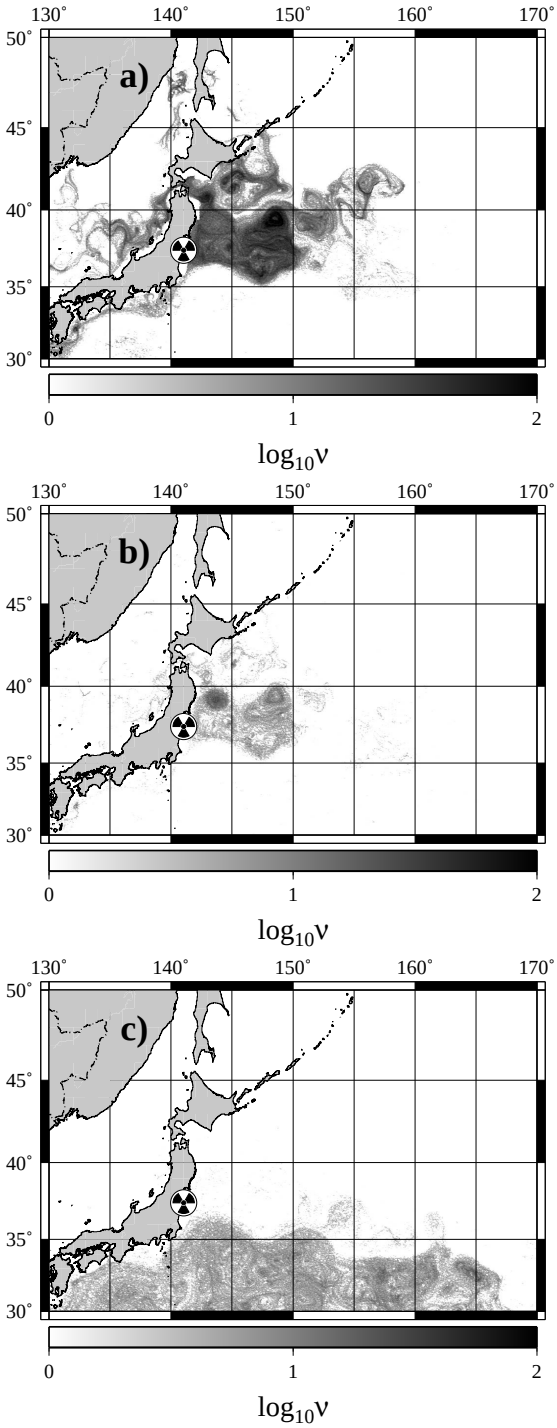

Figure 9: The same as in Fig. 8 but for the tracers distributed in the center of (a) the mesoscale eddy B at station 61, (b) the mesoscale eddy C at station 65 and (c) the mesoscale eddy D at station 69. The density of tracers, ν, is in a logarithmic scale.

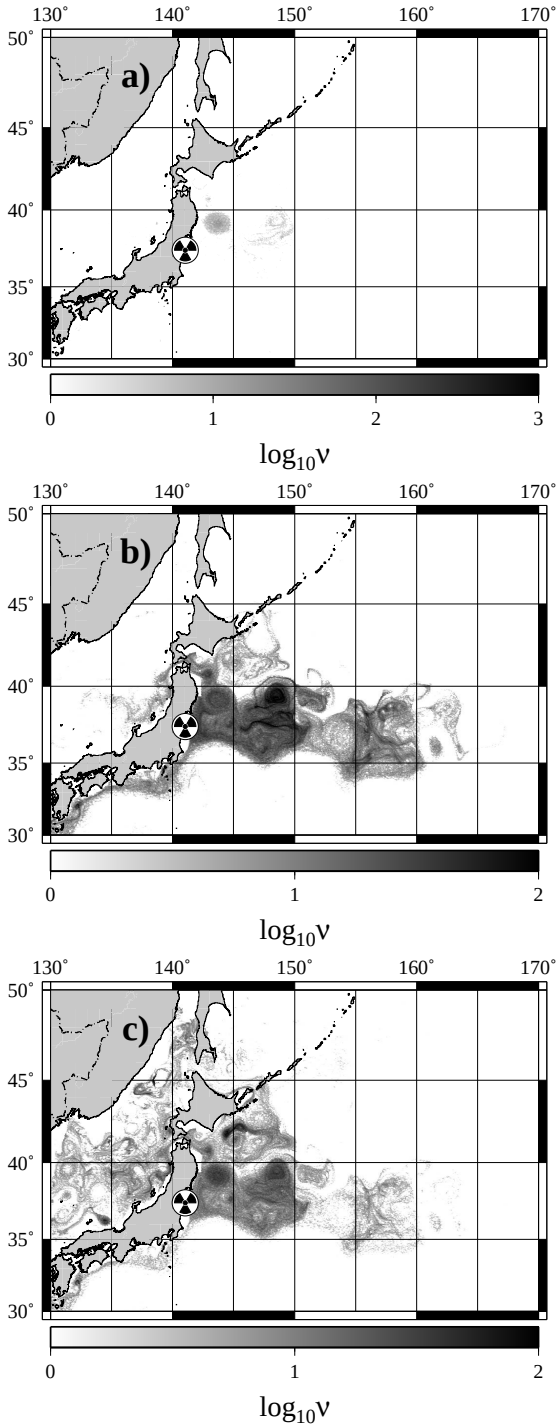

Figure 10: The same as in Fig. 8 but for the tracers distributed in the centers of (a) the mesoscale eddy E at station 74, (b) the mesoscale eddy F at station 79 and (c) the mesoscale eddy G at station 84. The density of tracers, ν, is in a logarithmic scale.

to be the most intense dynamic feature among the sampled eddies. Isopycnes of 26.8–27.6 are deepened in its center by 450–550 m as compared with surrounding water. Another energetic eddies are the Kuroshio warm-core rings D and G.

Distribution of potential vorticity (Fig. 5b) indicates an existence of low potential vorticity layers in the centers of eddies A, B, C and G in the depth range of 50–750 m. This corresponds to well mixed vertically uniform cores of the eddies formed during eddy evolution (Kitano, 1975; Lobanov et al., 1991; Itoh and Yasuda, 2010b). Vertical mixing, driven by winter convection, contributes to the formation of eddy cores. Thus, the older eddies have larger and less stratified cores. In opposite, relatively young eddies do not have a uniform layer in their centers. An absence of any noticeable well mixed layer in the eddies D, E, and F confirms their relatively young age detected by satellite altimetry and our modeling results. The relatively old Kuroshio warm-core ring G demonstrated a more complicated structure having two low potential vorticity layers. The upper one, corresponding to warm and higher salinity core of the eddy, is located between 55 and 205 m (Figs. 3s and 4s). While the secondary core of the eddy, formed by lower temperature and salinity waters subducted into the eddy center, is located at 410–750 m. Low potential vorticity cores of the eddies A, B, C and G also have a high content of dissolved oxygen (Fig. 5s) which indicates recent ventilation of these waters. Considering these features of the eddy structure, we may expect accumulation of surface water with radionuclides in the centers of anticyclonic eddies and vertical transport of this water downward in the eddy cores.

Distribution of ^{134}Cs and ^{137}Cs concentrations in surface waters along the cruise track in the Pacific (Fig. 6) shows increased cesium content in the areas of stations 56–65 and stations 81–84 corresponding to the northern subarctic front areas along 155° E and to the south-east off Hokkaido. Maximal concentrations are observed in the mesoscale eddy B located at the northern subarctic front with ^{134}Cs and ^{137}Cs contents at station 61 up to 11.9 and 21.0 Bq m^{-3}, respectively (Table 1). High concentration of both the cesium isotopes were also observed at the southern periphery of the mesoscale eddy B at station 63 (9.7 and 16.6 Bq m^{-3}) and in the area of the mesoscale eddy G at station 84 (6.1 and 11.8 Bq m^{-3}). This suggests a direct transport of water enriched by radionuclides from the Fukushima area by streamers and its trapping in those eddies that corresponds well with our modeling results.

The observed concentrations of cesium were low at the southern part of our transect (stations 70–79) within the surface layers of the eddies D, E, and F, influenced by relatively clean water transported by the Kuroshio Extension. In the area to the north of the subarctic front and the central Kuril Islands (the eddy A), again we have not found a high content of radiocesium. Concentrations of ^{134}Cs and ^{137}Cs at stations 45–50 in the area of the eddy A were around 0.4–1.2 and 1.7–3.7 Bq m^{-3} which is higher than in the Japan and Okhotsk Seas. However, this is rather a result of atmospheric deposition then direct advection by water flow.

Vertical distribution of radiocesium, sampled at some stations, is shown in Fig. 7. Inside most of the eddies a higher concentration is observed not at the surface but withim subsurface layers deepened down to 200–500 m. The maximal content of cesium isotopes in the eddies B, C and G (stations 61, 65 and 84) is observed in the low vorticity cores of these eddies located around 200, 200 and 100 m, correspondingly (Fig. 5b). This proves our preliminary hypothesis that water with Fukushima-derived radionuclides was subducted and trapped in the cores of anticyclonic eddies. Lower content of cesium at surface layer of the eddies may be explained by a faster ventilation of surface layer by mesoscale streamers and advection of relatively clean water originated from the Kuroshio Extension.

Our observations show that maximal concentrations of cesium in the subarctic frontal zone in June – July 2012 was located not at the surface but within subsurface and intermediate water layers in the potential density range of 26.5–26.7 σ_θ. Deepening of these isopycnal surfaces in anticyclonic eddies resulted in deeper locations of radionuclide maxima. Thus, high concentrations of cesium were observed down to 300–400 m in the eddies F, E and G (stations 75, 79 and 84) and down to 500 m in the mesoscale eddy D (station 69). Even deeper penetration of ^{134}Cs and ^{137}Cs, down to 1000 m, was observed in the mesoscale eddy B (station 61) of 0.8 ± 0.2 and 1.9 ± 0.2 Bq m^{-3}.

The first observations of vertical distribution of Fukushima-derived cesium, taken in summer of 2011 (e.g., Buesseler et al., 2012), found increased content of cesium isotope at the upper surface layer down to 50–100 m. Then, starting from spring 2012 and later, a higher concentration of cesium was observed subducted down to subsurface

and intermediate layers (Kaeriyama et al., 2014; Kumamoto et al., 2014). This coincides well with our results which show that subduction in the frontal zone forms a cesium enriched intermediate water which then spreads southward at the depth of 200–370 m between potential density anomalies surfaces of 25.20–25.33 as North Pacific Subtropical Mode Water (Kumamoto et al., 2014). Modeling results by (Rossi et al., 2013) also demonstrate deep penetration of radiocesium rich water into the North Pacific Mode Water in the eastern areas of the North Pacific. We demonstrate that on the background of this large-scale subduction and advection anticyclonic mesoscale eddies could be considered as an effective mechanism of downward transport and advection of cesium-rich water. Our observations prove that high radiocesium concentrations are observed exactly inside the uniform core of the eddies (termostad) located in the density range 26.5–26.7 which corresponds to the North Pacific Intermediate Water forming in the subarctic frontal zone area (Talley et al., 1995; Shimizu et al.). Thus, we expect that the eddies can trap this water with the maximal content of radiocesium and transport it horizontally and vertically. Considering the northward translation of the eddies, we may suggest that Fukushima-derived cesium should be also transported by the eddies to the north at the intermediate depth.

4.4. Backward-in-time tracking maps for samples collected at stations in the centers of anticyclonic eddies of the subarctic front

In this section we present the results of numerical simulation with tracers distributed in the centers of the eddies A, B, C, D, E, F and G where seawater samples were collected at some cruise stations. All the tracking experiments here have been performed backward in time for each mesoscale eddy to be studied. Starting from the day of sampling in the center of the corresponding eddy, synthetic tracers have been advected backward in time till the day of the tsunami, 11 March 2011. Fixing the places, where they have been for the month after the accident, from 11 March to 10 April 2011, we plot the corresponding map.

Station 50 (154.33° E; 46.19° N) was located near the elliptic point of the mesoscale eddy A, which is a Kuril anticyclone with the size $\simeq 3^\circ \times 1.5^\circ$ located approximately at the same place from the day of the accident (and even earlier) to the end of the cruise (and even later). The observed concentrations at different depths (see Table) ranged for ^{137}Cs from 0.6 ± 0.1 to 1.7 ± 0.3 Bq m^{-3} and did not exceed the background level. It is seen in Fig. 8a that the tracers of station 50 have not visited the latitudes to the south off 40° N where one would expect a significant contamination due to the accident. We may conclude that the probability to detect an increased cesium concentration in the eddy A is small. For comparison, we computed in Fig. 8b a tracking map for tracers of station 56 (155° E; 44.05° N) located outside any eddy. The observed concentration of ^{137}Cs in surface water samples at that station, 5.9 ± 0.5 Bq m^{-3}, exceeds the background level more than in three times. The traces of simulated particles in Fig. 8b are found to be closer to the FNPP location than the tracers in Fig. 8a (please, pay attention that the concentration in those figures is in a logarithmic scale).

Station 61 (154.4° E; 41.9° N) was located near the elliptic point of the mesoscale eddy B with the size $\simeq 1.5^\circ \times 1.5^\circ$. The highest cesium concentrations, 21.1 ± 1.1 at surface and 21.6 ± 0.9 Bq m^{-3} at 203 m depth, have been observed in seawater samples at that station. Our observations are agreed with measurements by Kaeriyama et al. (2013) to be carried out approximately at the same place and in the same period. They detected the concentration of ^{137}Cs in surface seawater samples, 18 ± 0.7 Bq m^{-3}, at their station B38 located nearby our station 61 and 17 ± 0.7 Bq m^{-3} and 13 ± 0.7 Bq m^{-3} at stations B37 and B39 located inside the eddy B. The tracking map in Fig. 9a shows that tracers of the eddy B have visited for the month after the accident the area with presumably high level of contamination. In particular, they have visited frequently the location of the Tohoku eddy T in March and April 2011 with the highest levels of cesium concentration (besides the FNPP discharge channels) to be detected just after the accident (Kaeriyama et al., 2013). We traced out the history of the mesoscale eddy B and found that it was born on the southern flank of a zonal eastward jet transporting waters from the eastern coast of Japan. That jet is seen on the computed zonal drift Lagrangian map in Fig. 3d as a wave-like grey (red online) band extending approximately along 42–43° N. Red (blue) colors mean that the corresponding tracers passed for the integration time (15 days) large distances in the west – east and the east – west directions, respectively.

Station 65 (154° E; 39.75° N) was located near the elliptic point of the mesoscale eddy C with the

size $\simeq 1^\circ \times 1^\circ$, which was born in January 2012 as a companion of the warm-core Kuroshio Extension ring D. The high concentration of ^{137}Cs, 22.7 ± 1.5 Bq m^{-3}, has been detected at 200 m depth, whereas it was relatively low at the surface and at 500 and 1000 m depths (see Table). The concentrations of ^{137}Cs in surface seawater samples at Japanese stations A34 and A33, located nearby our station 65, and at station A35 located in the core of the eddy C were found by (Kaeriyama et al., 2013) to be relatively high, 9.2 ± 0.5, 11 ± 0.6 and 13 ± 0.7 Bq m^{-3}. The probability that waters of the eddy C could contain a large amount of Fukushima-derived radionuclides is comparatively high because the tracers in Fig. 9b have frequently visited the contaminated area and, in particular, the Tohoku eddy T.

The Kuroshio ring D with the size $\simeq 2.5^\circ \times 3^\circ$ was pinched off from a meander of the Kuroshio Extension jet in the end of May 2012. Until the middle of August it was a free ring sometimes to be connected with the parent jet by an arch. The probability to detect higher concentrations of cesium in its surface water is estimated to be low (see Fig. 9c) because it contains mainly Kuroshio waters. We have detected in surface water samples the concentration of ^{137}Cs to be 6.3 ± 0.4 Bq m^{-3}. It is greater than the background level that may be explained by water exchange with its companion, the mesoscale eddy C with a high level of radioactivity. The concentrations of ^{137}Cs in surface seawater samples at Japanese stations B30, located closely to our station 69, and at station B29, located nearby our station 70, were found by (Kaeriyama et al., 2013) to be slightly greater the background level, 3.6 ± 0.5 and 3.4 ± 0.4 Bq m^{-3}, respectively.

The Kuroshio ring E with the size $\simeq 1.5^\circ \times 1^\circ$ was pinched off from a meander of the jet on 10–12 June 2012 and disappeared in the middle of July. Station 74 (151.5° E; 38.38° N) was located near the elliptic point of that eddy where the increased concentration of ^{137}Cs, 12.3 ± 0.8 Bq m^{-3}, has been detected at 307 m depth. A comparatively small number of tracers over the whole broad area in Fig. 10a is explained by the history of core waters in the mesoscale eddy E which have been transported mainly by the Kuroshio from the south and then directed to the east by the Kuroshio Extension. The genesis of the eddy E shows a presence of the Tohoku eddy waters in its core (see the patch in Fig. 10a centered at ≈143° E; 39° N).

The mesoscale eddy F with the size $\simeq 1^\circ \times 1^\circ$ has not been identified as a ring pinched off from the Kuroshio Extension. Station 79 (149.5° E; 39.5° N) was located near the elliptic point of that eddy where the increased concentrations of ^{137}Cs, ranged from 7.3 ± 0.7 to 9 ± 0.9 Bq m^{-3}, have been detected from the surface to 280 m depth. The tracking map in Fig. 10b demonstrates that water from its core really have visited potentially contaminated area around the FNPP location during the first month after the accident.

Station 84 (147.3° E; 41.3° N) was located near the elliptic point of the mesoscale eddy G with the size $\simeq 2^\circ \times 1.5^\circ$ situated at the traverse of the Tsugaru Strait. The tracking map for that station in Fig. 10c reveals its close connection with the Tohoku eddy T, and, therefore, the probability to detect increased cesium concentrations was expected to be comparatively large. In reality we detected the concentration of ^{137}Cs at 100 m depth to be as largr as 18 ± 1.3 Bq m^{-3}.

5. Conclusion

Results of observations of ^{134}Cs and ^{137}Cs, released from the Fukushima Nuclear Power Plant in seawater samples and collected at surface and different depths in the western North Pacific in June and July 2012 in the cruise of R/V "Professor Gagarinskiy", have demonstrated a background or slightly increased level of radiocesium in the Japan and Okhotsk seas and increased concentrations in the area of the subarctic front east of Japan. The highest concentrations of ^{134}Cs and ^{137}Cs (13.5 ± 0.9 and 22.7 ± 1.5 Bq m^{-3}) have been found to exceed ten times the background levels before the accident. Maximal content of radiocesium was observed inside the mesoscale anticyclonic eddies. Among the sampled eddies, the anticyclonic ring of the northern subarctic front B and the Kuroshio warm-core ring G (located south-east of Hokkaido) presented the highest concentration of cesium.

The maximal concentration of radionuclides was observed not at the surface but within subsurface and intermediate water layers (100 – 500 m) in the potential density range of 26.5 – 26.7 with extremely high values inside the low potential vorticity cores of the eddies B, C and G. This suggests that convergence and subduction of surface water inside eddies are main mechanisms of downward transport of radionuclides. In particular, in the eddies B and D a slightly increased content of radiocesium was observed even at depth of 1000 m. Con-

centrations of radiocesium in the eddies, located closer to the Kuroshio Extension (D, E and F), have been found to be very low at surface layer. It may be explained by a faster ventilation of surface layer by mesoscale streamers and advection of relatively clean water originated from the Kuroshio Extension. A higher content of radiocesium observed at 300–500 m depth was a result of sudbuction in the frontal zone and the following advection of intermediate water by the eddies.

The direct observations were compared with simulation of advection of these radioisotopes by the AVISO altimetric velocity field. Synthetic tracers, released at the locations of a number of stations inside the eddies, have been advected backward in time till the day of the accident. Fixing their traces for the month after the accident, we computed tracking maps for each of those stations which were used to reconstruct the history and origin of the tracers imitating measured seawater samples. Those maps allowed to explain why measured activities of ^{134}Cs and ^{137}Cs differed strongly in different samples. It has been shown that tracers with increased radioactivity really have visited the areas with presumably high level of contamination just after the accident. In particular, it has been found a close connection of the samples with increased radioactivity in the eddies B, C, E, F and G with the Tohoku eddy T known to be strongly contaminated just after the accident (Honda et al., 2012; Buesseler et al., 2012; Kaeriyama et al., 2013).

Thus, the eddies play an important role in the transport of water with radionuclides released from the FNPP. Considering subduction and accumulation of high-cesium-content water in the anticyclonic eddies, we may suggest that Fukushima-derived cesium should be also transported by the eddies northward at the intermediate depth.

Supplementary material related to this paper is available online.

Acknowledgments

The authors would like to thank the research team and crew of R/V “Professor Gagarinskiy” for their hard work at sea. The cruise was supported by the Far Eastern Branch of Russian Academy of Sciences and the Russian Foundation for Basic Research (the expedition grant 11–05–02110). The modeling work was supported by the Russian Foundation for Basic Research (project nos. 12–05–00452, 13–05–00099 and 13–01–12404). The altimeter products were distributed by AVISO with support from CNES.

Station	Time	Longitude	Latitude	Depth, m	Temp, °C	Sal, psu	^{134}Cs, Bq/m^3	^{137}Cs, Bq/m^3
1	12.06.12 13:50	131.877° E	43.067° N	0	12.401	32.117	< 0.09	1.9 ± 0.2
7	14.06.12 01:56	131.995° E	42.514° N	0	9.700	33.860	< 0.08	1.7 ± 0.2
11	14.06.12 11:55	132.004° E	42.220° N	0	10.390	33.850	< 0.08	1.9 ± 0.3
16	15.06.12 14:18	132.517° E	40.668° N	0	15.198	33.972	< 0.05	1.4 ± 0.2
				201	1.454	33.978	< 0.07	1.7 ± 0.3
				751	0.533	34.069	< 0.07	1.7 ± 0.3
				1500	0.195	34.066	< 0.08	0.7 ± 0.1
				2500	0.110	34.065	< 0.06	0.4 ± 0.1
				3361	0.090	34.065	< 0.09	1.0 ± 0.3
21	16.06.12 21:21	133.167° E	40.003° N	0	17.607	34.000	< 0.07	2.2 ± 0.3
24	17.06.12 19:09	133.997° E	41.504° N	0	14.609	33.950	< 0.08	1.6 ± 0.2
25	18.06.12 05:01	135.121° E	41.520° N	0	14.370	33.880	< 0.05	2.0 ± 0.2
				2900	0.087	34.064	< 0.06	0.3 ± 0.1
26	18.06.12 12:00	135.722° E	41.847° N	0	14.657	33.852	< 0.08	1.6 ± 0.2
27	19.06.12 07:08	137.183° E	42.818° N	0	15.212	33.908	< 0.07	2.2 ± 0.2
				3621	0.088	34.065	< 0.06	1.1 ± 0.1
28	19.06.12 15:15	137.842° E	43.501° N	0	15.690	33.967	< 0.09	2.3 ± 0.3
29	20.06.12 01:21	138.696° E	44.311° N	0	15.306	34.030	< 0.08	2.0 ± 0.2
L2	21.06.12 01:30	141.408° E	45.721° N	0	11.980	33.806	0.3 ± 0.2	2.4 ± 0.3
L3	21.06.12 08:00	142.110° E	45.686° N	0	9.045	33.540	< 0.08	1.8 ± 0.2
L4	21.06.12 14:00	142.935° E	45.737° N	0	8.918	32.203	< 0.06	1.5 ± 0.2
L5	21.06.12 20:30	144.024° E	45.805° N	0	8.355	32.242	< 0.06	1.5 ± 0.2
30	22.06.12 08:16	146.076° E	45.934° N	0	8.206	32.281	< 0.03	1.5 ± 0.1
				150	-0.340	33.180	< 0.07	1.4 ± 0.1
				500	1.560	33.640	< 0.03	1.1 ± 0.1
				1005	2.220	34.240	< 0.07	0.9 ± 0.2
				2200	1.785	34.506	< 0.03	0.7 ± 0.1
				3236	1.626	34.604	< 0.07	0.4 ± 0.1
31	23.06.12 07:43	148.393° E	46.456° N	0	8.591	32.272	< 0.05	1.6 ± 0.1
35	24.06.12 05:36	150.932° E	47.043° N	0	5.810	32.640	< 0.06	1.5 ± 0.1
43	24.06.12 23:11	151.609° E	46.204° N	0	3.843	32.976	0.4 ± 0.1	1.9 ± 0.5
44	25.06.12 10:57	152.732° E	47.050° N	0	6.010	32.910	0.9 ± 0.2	2.6 ± 0.2
45	25.06.12 15:16	153.095° E	46.803° N	0			1.2 ± 0.2	3.7 ± 0.4
				200			0.4 ± 0.1	1.9 ± 0.2
				500			< 0.07	0.9 ± 0.1
				1000			< 0.08	0.7 ± 0.1
49	26.06.12 12:10	154.577° E	46.083° N	0	6.700	33.030	0.4 ± 0.1	1.8 ± 0.2
50	26.06.12 14:54	154.334° E	46.197° N	200	1.320	33.360	0.5 ± 0.2	1.7 ± 0.3
				500	1.680	33.460	0.2 ± 0.1	1.5 ± 0.1
				1000	3.240	34.150	< 0.03	0.6 ± 0.1
54	27.06.12 08:03	155.279° E	45.717° N	0	6.501	32.932	1.2 ± 0.1	3.0 ± 0.3
56	27.06.12 23:05	155.000° E	44.050° N	0	7.256	33.011	3.0 ± 0.3	5.9 ± 0.5
				200	2.932	33.573	0.5 ± 0.2	2.0 ± 0.2
				500	3.334	34.122	< 0.09	0.9 ± 0.1
				1000	2.554	34.404	< 0.07	0.5 ± 0.1

Station	Time	Longitude	Latitude	Depth, m	Temp, °C	Sal, psu	^{134}Cs, Bq/m^3	^{137}Cs, Bq/m^3
				2002	1.705	34.601	< 0.06	0.4 ± 0.1
				3002	1.297	34.661	< 0.09	0.5 ± 0.3
58	28.06.12 17:27	155.005° E	42.999° N	0	12.800	34.020	2.4 ± 0.2	5.2 ± 0.4
61	29.06.12 06:30	154.438° E	41.936° N	0	11.580	33.985	11.9 ± 0.6	21.0 ± 1.1
				203	6.817	33.904	12.5 ± 0.5	21.6 ± 0.9
				500	4.135	33.907	0.2 ± 0.1	1.6 ± 0.3
				1000	3.064	34.347	0.8 ± 0.2	1.9 ± 0.2
63	29.06.12 18:15	154.262° E	41.068° N	0	12.100	33.940	9.7 ± 0.5	16.6 ± 0.9
65	30.06.12 06:42	154.003° E	39.750° N	0	17.139	34.444	2.1 ± 0.2	4.8 ± 0.3
				200	9.218	34.155	13.5 ± 0.9	22.7 ± 1.5
				500	5.017	33.926	< 0.07	0.9 ± 0.2
				1000	3.173	34.354	< 0.11	0.7 ± 0.2
69	01.07.12 08:44	154.001° E	37.842° N	0	18.650	34.690	2.8 ± 0.2	6.3 ± 0.4
				205	15.990	34.630	4.1 ± 0.3	8.0 ± 0.5
				500	7.770	34.030	3.5 ± 0.3	7.2 ± 0.6
				1000			< 0.07	1.1 ± 0.2
70	01.07.12 20:25	153.981° E	37.366° N	0	22.368	34.390	0.2 ± 0.1	2.3 ± 0.2
71	02.07.12 06:15	152.813° E	37.863° N	0	18.304	34.313	1.6 ± 0.2	4.5 ± 0.3
74	02.07.12 19:24	151.536° E	38.385° N	0	19.120	34.518	0.6 ± 0.1	2.5 ± 0.2
				100	14.860	34.530	1.1 ± 0.2	4.0 ± 0.4
				307	5.893	33.885	5.6 ± 0.6	12.3 ± 0.8
				500	4.720	34.021	< 0.07	1.4 ± 0.1
76	03.07.12 09:56	150.701° E	38.836° N	0	18.650	34.235	< 0.06	0.4 ± 0.1
77	03.07.12 16:37	150.002° E	39.151° N	0	18.290	34.370	1.5 ± 0.2	4.1 ± 0.3
79	04.07.12 02:41	149.003° E	39.495° N	0	18.174	34.319	1.7 ± 0.2	4.3 ± 0.3
				100	10.643	34.236	2.9 ± 0.4	7.3 ± 0.7
				280	3.906	33.489	3.5 ± 0.6	9.0 ± 0.9
				500	4.229	33.964	< 0.05	1.3 ± 0.2
81	04.07.12 14:54	148.387° E	40.234° N	0	15.950	33.530	3.1 ± 0.3	6.7 ± 0.5
82	04.07.12 20:20	147.996° E	40.631° N	0	13.625	33.242	1.0 ± 0.1	2.5 ± 0.2
84	05.07.12 05:29	147.329° E	41.299° N	0	14.750	33.846	6.1 ± 0.4	11.0 ± 0.6
				100	8.352	33.979	10.4 ± 0.7	18.0 ± 1.3
				350	4.672	33.601	6.9 ± 0.4	11.3 ± 0.6
				500	1.895	33.432	0.4 ± 0.1	1.7 ± 0.2

Table 1: Concentrations of ^{134}Cs and ^{137}Cs in seawater collected in the western North Pacific including the Japan and Okhotsk Seas.

References

Aoyama, M., Uematsu, M., Tsumune, D., Hamajima, Y., 2013. Surface pathway of radioactive plume of TEPCO Fukushima NPP1 released ^{134}Cs and ^{137}Cs. Biogeosciences 10, 3067–3078. doi:10.5194/bg-10-3067-2013.

Bandong, B.B., Volpe, A.M., Esser, B.K., Bianchini, G.M., 2001. Pre-concentration and measurement of low levels of gamma-ray emitting radioisotopes in coastal waters. Applied Radiation and Isotopes 55, 653–665. doi:10.1016/s0969-8043(01)00081-1.

Behrens, E., Schwarzkopf, F.U., Lübbecke, J.F., Büning, C.W., 2012. Model simulations on the long-term dispersal of ^{137}Cs released into the Pacific Ocean off Fukushima. Environmental Research Letters 7, 034004. doi:10.1088/1748-9326/7/3/034004.

Buesseler, K.O., Jayne, S.R., Fisher, N.S., Rypina, I.I., Baumann, H., Baumann, Z., Breier, C.F., Douglass, E.M., George, J., Macdonald, A.M., Miyamoto, H., Nishikawa, J., Pike, S.M., Yoshida, S., 2012. Fukushima-derived radionuclides in the ocean and biota off Japan. Proceedings of the National Academy of Sciences 109, 5984–5988. doi:10.1073/pnas.1120794109.

Bulatov, N.V., Lobanov, V.B., 1992. Influence of the Kuroshio warm-core rings on hydrographic and fishery conditions off Southern Kuril Islands, in: Proceedings of the PORSEC-92 in Okinawa, pp. 1127–1131.

Choi, Y., Kida, S., Takahashi, K., 2013. The impact of oceanic circulation and phase transfer on the dispersion of radionuclides released from the Fukushima Daiichi Nuclear Power Plant. Biogeosciences 10, 4911–4925. doi:10.5194/bg-10-4911-2013.

Dianskii, N.A., Gusev, A.V., Fomin, V.V., 2012. The specific features of pollution spread in the northwest Pacific Ocean. Izvestiya, Atmospheric and Oceanic Physics 48, 222–240. doi:10.1134/s0001433812010033.

Dietze, H., Kriest, I., 2012. ^{137}Cs off Fukushima Dai-ichi, Japan — model based estimates of dilution and fate. Ocean Science 8, 319–332. doi:10.5194/os-8-319-2012.

Haller, G., 2000. Finding finite-time invariant manifolds in two-dimensional velocity fields. Chaos: An Interdisciplinary Journal of Nonlinear Science 10, 99–108. doi:10.1063/1.166479.

Honda, M.C., Aono, T., Aoyama, M., Hamajima, Y., Kawakami, H., Kitamura, M., Masumoto, Y., Miyazawa, Y., Takigawa, M., Saino, T., 2012. Dispersion of artificial caesium-134 and -137 in the western North Pacific one month after the Fukushima accident. Geochemical Journal 46, e1–e9.

Inoue, M., Kofuji, H., Hamajima, Y., Nagao, S., Yoshida, K., Yamamoto, M., 2012a. ^{134}Cs and ^{137}Cs activities in coastal seawater along Northern Sanriku and Tsugaru Strait, northeastern Japan, after Fukushima Dai-ichi Nuclear Power Plant accident. Journal of Environmental Radioactivity 111, 116–119. doi:10.1016/j.jenvrad.2011.09.012.

Inoue, M., Kofuji, H., Nagao, S., Yamamoto, M., Hamajima, Y., Yoshida, K., Fujimoto, K., Takada, T., Isoda, Y., 2012b. Lateral variation of ^{134}Cs and ^{137}Cs concentrations in surface seawater in and around the Japan Sea after the Fukushima Dai-ichi Nuclear Power Plant accident. Journal of Environmental Radioactivity 109, 45–51. doi:10.1016/j.jenvrad.2012.01.004.

Itoh, S., Yasuda, I., 2010a. Characteristics of mesoscale eddies in the Kuroshio – Oyashio Extension region detected from the distribution of the sea surface height anomaly. Journal of Physical Oceanography 40, 1018–1034. doi:10.1175/2009JPO4265.1.

Itoh, S., Yasuda, I., 2010b. Water mass structure of warm and cold anticyclonic eddies in the western boundary region of the Subarctic North Pacific. Journal of Physical Oceanography 40, 2624–2642. doi:10.1175/2010jpo4475.1.

Kaeriyama, H., Ambe, D., Shimizu, Y., Fujimoto, K., Ono, T., Yonezaki, S., Kato, Y., Matsunaga, H., Minami, H., Nakatsuka, S., Watanabe, T., 2013. Direct observation of ^{134}Cs and ^{137}Cs in surface seawater in the western and central North Pacific after the Fukushima Dai-ichi nuclear power plant accident. Biogeosciences 10, 4287–4295. doi:10.5194/bg-10-4287-2013.

Kaeriyama, H., Shimizu, Y., Ambe, D., Masujima, M., Shigenobu, Y., Fujimoto, K., Ono, T., Nishiuchi, K., Taneda, T., Kurogi, H., Setou, T., Sugisaki, H., Ichikawa, T., Hidaka, K., Hiroe, Y., Kusaka, A., Kodama, T., Kuriyama, M., Morita, H., Nakata, K., Morinaga, K., Morita, T., Watanabe, T., 2014. Southwest intrusion of ^{134}Cs and ^{137}Cs derived from the Fukushima Dai-ichi nuclear power plant accident in the western North Pacific. Environmental Science and Technology 48, 3120–3127. doi:10.1021/es403686v.

Kameník, J., Dulaiova, H., Buesseler, K.O., Pike, S.M., Šťastná, K., 2013. Cesium-134 and 137 activities in the central North Pacific Ocean after the Fukushima Dai-ichi Nuclear Power Plant accident. Biogeosciences 10, 6045–6052. doi:10.5194/bg-10-6045-2013.

Kanda, J., 2013. Continuing ^{137}Cs release to the sea from the Fukushima Dai-ichi Nuclear Power Plant through 2012. Biogeosciences 10, 6107–6113. doi:10.5194/bg-10-6107-2013.

Karasev, E.V., 2012. Monitoring of ecological conditions of the Far East seas, in: Proceedings of the 2nd International Meeting of Amur-Okhotsk consortium, Amur-Okhotsk Consortium. pp. 75–80. URL: http://amurokhotsk.com/wp-content/uploads/2012/04/Proceedings.pdf

Kawai, H., 1972. Hydrography of the Kuroshio Extension, in: Stommel, H., Yoshida, K. (Eds.), Kuroshio: Physical Aspects of the Japan Current. University of Washington Press, Seattle, pp. 235–352.

Kawamura, H., Kobayashi, T., Furuno, A., In, T., Ishikawa, Y., Nakayama, T., Shima, S., Awaji, T., 2011. Preliminary numerical experiments on oceanic dispersion of ^{131}I and ^{137}Cs discharged into the ocean because of the Fukushima Daiichi nuclear power plant disaster. Journal of Nuclear Science and Technology 48, 1349–1356. doi:10.1080/18811248.2011.9711826.

Kitano, K., 1974. A Kuroshio anticyclonic eddy. Journal of Physical Oceanography 4, 670–672. doi:10.1175/1520-0485(1974)004<0670:AKAE>2.0.CO;2.

Kitano, K., 1975. Some properties of the warm eddies generated in the confluence zone of the Kuroshio and Oyashio currents. Journal of Physical Oceanography 5, 245–352. doi:10.1175/1520-0485(1975)005<0245:SPOTWE>2.0.CO;2.

Kumamoto, Y., Aoyama, M., Hamajima, Y., Aono, T., Kouketsu, S., Murata, A., Kawano, T., 2014. Southward spreading of the Fukushima-derived radiocesium across the Kuroshio Extension in the North Pacific. Scientific Reports 4, 1–9. doi:10.1038/srep04276.

Lobanov, V.B., Rogachev, K.A., Bulatov, N.V., Lomakin, A.F., Tolmachev, K.P., 1991. Long-term evolution of the Kuroshio warm eddy. Doklady USSR Akademy of Sciences

317, 984–988. [in Russian].

Maderich, V., Bezhenar, R., Heling, R., de With, G., Jung, K., Myoung, J., Cho, Y.K., Qiao, F., Robertson, L., 2014. Regional long-term model of radioactivity dispersion and fate in the Northwestern Pacific and adjacent seas: application to the Fukushima Dai-ichi accident. Journal of Environmental Radioactivity 131, 4–18. doi:10.1016/j.jenvrad.2013.09.009.

Miyazawa, Y., Masumoto, Y., Varlamov, S.M., Miyama, T., Takigawa, M., Honda, M., Saino, T., 2013. Inverse estimation of source parameters of oceanic radioactivity dispersion models associated with the Fukushima accident. Biogeosciences 10, 2349–2363. doi:10.5194/bg-10-2349-2013.

Nakano, M., Povinec, P.P., 2012. Long-term simulations of the ^{137}Cs dispersion from the Fukushima accident in the world ocean. Journal of Environmental Radioactivity 111, 109–115. doi:10.1016/j.jenvrad.2011.12.001.

Oikawa, S., Takata, H., Watabe, T., Misonoo, J., Kusakabe, M., 2013. Distribution of the Fukushima-derived radionuclides in seawater in the Pacific off the coast of Miyagi, Fukushima, and Ibaraki prefectures, Japan. Biogeosciences 10, 5031–5047. doi:10.5194/bg-10-5031-2013.

Pierrehumbert, R.T., Yang, H., 1993. Global chaotic mixing on isentropic surfaces. Journal of the Atmospheric Sciences 50, 2462–2480. doi:10.1175/1520-0469(1993)050<2462:GCMOIS>2.0.CO;2.

Prants, S., Budyansky, M., Ponomarev, V., Uleysky, M., 2011a. Lagrangian study of transport and mixing in a mesoscale eddy street. Ocean Modelling 38, 114–125. doi:10.1016/j.ocemod.2011.02.008.

Prants, S., Budyansky, M., Uleysky, M., 2014a. Identifying Lagrangian fronts with favourable fishery conditions. Deep Sea Research Part I: Oceanographic Research Papers 90, 27–35. doi:10.1016/j.dsr.2014.04.012.

Prants, S.V., 2013. Dynamical systems theory methods to study mixing and transport in the ocean. Physica Scripta 87, 038115. doi:10.1088/0031-8949.

Prants, S.V., Budyansky, M.V., Uleysky, M.Y., 2014b. Lagrangian study of surface transport in the Kuroshio Extension area based on simulation of propagation of Fukushima-derived radionuclides. Nonlinear Processes in Geophysics 21, 279–289. doi:10.5194/npg-21-279-2014.

Prants, S.V., Ponomarev, V.I., Budyansky, M.V., Uleysky, M.Y., Fayman, P.A., 2013. Lagrangian analysis of mixing and transport of water masses in the marine bays. Izvestiya, Atmospheric and Oceanic Physics 49, 82–96. doi:10.1134/S0001433813010088.

Prants, S.V., Uleysky, M.Y., Budyansky, M.V., 2011b. Numerical simulation of propagation of radioactive pollution in the ocean from the Fukushima Dai-ichi nuclear power plant. Doklady Earth Sciences 439, 1179–1182. doi:10.1134/S1028334X11080277.

Prants, S.V., Uleysky, M.Y., Budyansky, M.V., 2012. Lagrangian coherent structures in the ocean favorable for fishery. Doklady Earth Sciences 447, 1269–1272. doi:10.1134/S1028334X12110062.

Remez, V., 1996. The application of caesium selective sorbents in the remediation and restoration of radioactive contaminated sites, in: Luykx, F., Frissel, M. (Eds.), Radioecology and the Restoration of Radioactive-Contaminated Sites. Springer Netherlands. volume 13 of *NATO ASI Series*, pp. 217–224. doi:10.1007/978-94-009-0301-2_17.

Remez, V., Sapozhnikov, Y., 1996. The rapid determination of caesium radionuclides in water systems using composite sorbents. Applied Radiation and Isotopes 47, 885–886. doi:10.1016/s0969-8043(96)00080-2.

Rossi, V., Sebille, E.V., Gupta, A.S., Garçon, V., England, M.H., 2013. Multi-decadal projections of surface and interior pathways of the Fukushima Cesium-137 radioactive plume. Deep Sea Research Part I: Oceanographic Research Papers 80, 37–46. doi:10.1016/j.dsr.2013.05.015.

Rypina, I.I., Jayne, S.R., Yoshida, S., Macdonald, A.M., Douglass, E., Buesseler, K., 2013. Short-term dispersal of Fukushima-derived radionuclides off Japan: modeling efforts and model-data intercomparison. Biogeosciences 10, 4973–4990. doi:10.5194/bg-10-4973-2013.

Shimizu, Y., Iwao, T., Yasuda, I., Ito, S.I., Watanabe, T., Uehara, K., Shikama, N., Nakano, T., . Formation process of North Pacific intermediate water revealed by profiling floats set to drift on 26.7 σ_θ isopycnal surface. Journal of Oceanography 60, 453–462. doi:10.1023/b:joce.0000038061.55914.eb.

Takemura, T., Nakamura, H., Takigawa, M., Kondo, H., Satomura, T., Miyasaka, T., Nakajima, T., 2011. A numerical simulation of global transport of atmospheric particles emitted from the Fukushima Daiichi nuclear power plant. SOLA 7, 101–104. doi:10.2151/sola.2011-026.

Talley, L.D., Nagata, Y., Fujimura, M., Iwao, T., Kono, T., Inagake, D., Hirai, M., Okuda, K., 1995. North Pacific intermediate water in the Kuroshio/Oyashio mixed water region. Journal of Physical Oceanography 25, 475–501. doi:10.1175/1520-0485(1995)025<0475:npiwit>2.0.co;2.

Tsumune, D., Tsubono, T., Aoyama, M., Hirose, K., 2012. Distribution of oceanic ^{137}Cs from the Fukushima Dai-ichi Nuclear Power Plant simulated numerically by a regional ocean model. Journal of Environmental Radioactivity 111, 100–108. doi:10.1016/j.jenvrad.2011.10.007.

Tsumune, D., Tsubono, T., Aoyama, M., Uematsu, M., Misumi, K., Maeda, Y., Yoshida, Y., Hayami, H., 2013. One-year, regional-scale simulation of ^{137}Cs radioactivity in the ocean following the Fukushima Dai-ichi Nuclear Power Plant accident. Biogeosciences 10, 5601–5617. doi:10.5194/bg-10-5601-2013.

Yasuda, I., Ito, S.I., Shimizu, Y., Ichikawa, K., Ueda, K.I., Honma, T., Uchiyama, M., Watanabe, K., Sunou, N., Tanaka, K., Koizumi, K., 2000. Cold-core anticyclonic eddies south of the Bussol' Strait in the Northwestern Subarctic Pacific. Journal of Physical Oceanography 30, 1137–1157. doi:10.1175/1520-0485(2000)030<1137:CCAESO>2.0.CO;2.

Yasuda, I., Okuda, K., Hirai, M., 1992. Evolution of a Kuroshio warm-core ring — variability of the hydrographic structure. Deep Sea Research Part A. Oceanographic Research Papers 39, S131–S161. doi:10.1016/s0198-0149(11)80009-9.